Volume 281, number 1,2, 212–218 FEBS 09544 April 1991

ADONIS 0014579391002600

# Conformation of endothelin in aqueous ethylene glycol determined by $^1$H-NMR and molecular dynamics simulations

Stanley R. Krystek, Jr.[1], Donna A. Bassolino[1], Jiri Novotny[1], Chinpan Chen[2], Thomas M. Marschner[2] and Niels H. Andersen[2]

[1]*Department of Macromolecular Modeling, Bristol-Myers Squibb Research Institute, Princeton, NJ 08543-4000, USA* and [2]*Department of Chemistry, University of Washington, Seattle, WA 98195, USA*

Received 18 December 1990; revised version received 24 January 1991

The solution conformation of a 21-residue vasoconstrictor peptide endothelin-1 (ET-1) in water-ethylene glycol has been determined by two-dimensional $^1$H-NMR spectroscopy and constrained molecular dynamics simulations. The N-terminus (residues 1–4) appears to undergo conformational averaging and no single structure consistent with the NMR constraints could be found for this region. Residues 5–8 form a turn, and residues 9–16 exist in a helical conformation. A flexible 'hinge' between residues 8–9 allows various orientations of the turn relative to the helix. Another 'hinge' at residue 17 connects the extended C-terminus to the bicyclic core region (residues 1–15). Residues important for binding and biological activity form a contiguous surface on one side of the helix, with the two disulfides extending from the other side of the helix.

Endothelin; NMR; Molecular dynamics; Three-dimensional structure

## 1. INTRODUCTION

In this communication, we summarize our recent NMR experiments and molecular dynamics simulation studies aimed at deriving the three-dimensional structure of endothelin-1 (ET-1) in aqueous ethylene glycol solution. ET-1, a 21-residue peptide with two disulfide bonds is a member of a new class of peptidic agents that includes mammalian endothelins and the sarafotoxin snake venom peptides [1,2]. Originally isolated from porcine endothelial cells [1], ET-1 has been shown to be a major endogenous vasoconstrictor in mammals [3]. ET-1 may also have other physiological or pathological functions, such as hemodynamic regulation and modulation of the cardiovascular system [3,4]. Increasing evidence for the involvement of endothelins in human disease has prompted a major effort in structural elucidation and pharmacological evaluation.

A hypothetical structural model of endothelin and circular dichroism measurements both suggested some degree of helicity [5]. Preliminary NMR studies [6,7] in aqueous solutions indicated a helical region between residues 9–15. The two different NMR structures proposed for ET-1 in dimethyl sulfoxide [8,9], are quite different and neither shows a regular helical region.

*Correspondence address:* S.R. Krystek Jr., Department of Macromolecular Modeling, Bristol-Myers Squibb Research Institute, PO Box 4000, Princeton, NJ 08543-4000, USA, *or* N.H. Anderson, Department of Chemistry, University of Washington, Seattle, WA 98195, USA. Fax: (1) (609) 683 6607

In this study a novel algorithm, DISCON (= DIStance CONstraints) [10], has been used to obtain experimental interproton distances with tighter bounds than those used in typical protein NMR studies [11]. The experimental distance constraints were then employed in three molecular dynamics programs (CONGEN, DISCOVER, and XPLOR) to derive models of the three-dimensional structure of ET-1. We found that portions of ET-1 have stable persistent structure, while other structural regions undergo conformational averaging. The persistently ordered regions include the side chains implicated in physiological function. In particular, our structural model identifies a contiguous surface area on the molecule that may be responsible for receptor binding.

## 2. EXPERIMENTAL

### 2.1. *Experimental methods*

Synthetic ET-1 was obtained from Penninsula Labs (Belmont, CA). NMR samples contained 1.5–3.2 mM of peptide in 60% v/v ethylene glycol-$d_6$/$H_2O$ with trifluoroacetic acid (2.5 mM) or $KH_2PO_4$/$K_2HPO_4$ (16 mM final). Samples in $D_2O$ media were obtained by repeated addition of 99.99% $D_2O$ and lyophilization. All NMR spectra were recorded at 500.145 MHz using Bruker instruments. Phase sensitive [12,13] NOESY spectra were collected and processed as previously described [14] with the following exceptions: all samples were spinning, and data was apodized using a skewed 60° shifted sine bell in both dimensions. Six separate experiments were carried out at 40–75% ethylene glycol, varying the mixing time, temperature and pH. TPPI-COSY spectra [15] were collected at each


*Published by Elsevier Science Publishers B.V.*

temperature and pH combination, typically 800–1024 $t_1$-values, 4K complex points in $t_2$.

For each spectrum, peak contour levels were recorded for all peaks (after a cubic spline baseplane correction) and a selection of cross-peaks and auto-peaks were also quantitated as volume integrals in order to evaluate peak height to volume factors. The DISCON algorithm [10] was applied to each NOESY volume intensity matrix in order to obtain experimental distances. Statistical comparisons over the 5 sets of experimental distances provided precision estimates which defined the bounds. Two types of constraints result: those with both low and high bounds, and those with only a low bound. The latter correspond to zero cross-peak intensities at specific resonance intersections.

### 2.2. *Computational methods*

Three-dimensional structures were generated from the NMR data using distance-constrained molecular dynamics calculations as implemented in the programs: CONGEN [16], DISCOVER (version 2.5, Biosym Technologies Inc.), and XPLOR (version 1.5, Polygen Corp.) running on Silicon Graphics 4D/20 or 4D/25 Personal Iris Workstations.

The 3 programs differed in their implementation of the distance constraint algorithm as well as the details of the empirical potential function parameterization (bond, angle and torsion force constants, atomic van der Waals radii, and partial atomic charges). XPLOR [17] uses a biharmonic potential with a variable force constant ($k_{NOE}$) such that $E_{NOE} = k_{NOE}$ (violation)$^2$. CONGEN, a modification of CHARMM [18], which includes a user-defined scale factor(s) and cutoff distance ($r_{max}$), uses a similar biharmonic potential when $r_{ij} < r_{max}$. In the region of $r_{ij} > r_{max}$ CONGEN employs $E_{NOE} = s(r_{ij} - r_{max})$ a skewed formula [19] for NOE constraints, such that large violations are scaled to a plateau. DISCOVER also uses a biharmonic potential for $r_{ij} < r_{max}$ and a skewed biharmonic function for $r_{ij} > r_{max}$:

$$E_{NOE} = c(2r_{ij} - r''_{ij} - r''_{max})(r''_{max} - r''_{ij}), \quad \text{if } r > r''_{max} \qquad [20]$$

where $r''_{max} = r''_{ij} + \text{force}_{max}/2c$ where $\text{force}_{max}$ is a user defined value for each constraint and $c = kTS/2\Delta^2$ ($k$ is the Boltzmann constant, $T$ is the absolute temperature, $S$ is the NOE scale factor and $\Delta$ is an error estimate). The skewed potential in CONGEN and DISCOVER allowed for inclusion of all constraints into a single set. The dynamics simulation protocol in CONGEN consisted of 50 ps of constant temperature dynamics (300K) with a NOE maximum force constant of 10.0 kcal·mol$^{-1}$·Å$^{-2}$ during the dynamics and a final NOE force constant of 2.0 kcal·mol$^{-1}$·Å$^{-2}$ during the 200 steps of conjugate gradient minimization which also effected disulfide closure. The DISCOVER procedure consisted of 50 ps molecular dynamics, which included 30 ps at the maximum temperature (900K). The NOE force constant at its maximum value was 89.4 kcal·mol$^{-1}$·Å$^{-2}$, the NOE force constant was 7.45 kcal·mol$^{-1}$·Å$^{-2}$ during the 200 steps of conjugate gradient minimization.

For XPLOR dynamics simulations [21] the interproton constraints were divided into six groups namely (1) well determined $d_{\alpha N}(i+1)$, $d_{\beta N}(i+1)$, $d_{NN}(i+1)$ connectivities and shorter $d_{\alpha N}(i)$, $d_{\alpha N}(i+3)$ and $d_{\alpha\beta}(i+3)$ connectivities; (2) other intra-residue connectivities and less well determined sequential $d_{\alpha N}$, $d_{NN}$ and $d_{\beta N}$ connectivities (i, i+n, n<4); (3) inter-residue connectivities across the disulfide linkages; (4) all constraints involving methyl groups; (5) all other intra-residue constraints; and (6) a set of distance constraints to accomplish disulfide closure and to favor the regular torsional angles ±90° for the CB-S-S-CB cystine side chain atoms. Molecular dynamics was carried out at 800K. Scale factors, initially set at 1.0 were uniformly increased by a factor of 1.15–1.60 every 30 fs until they reached the maximum values of 60 kcal·mol$^{-1}$·Å$^{-2}$ for constraint sets (3) to (6), and 100 kcal·mol$^{-1}$·Å$^{-2}$ for the constraint sets (1) and (2). The scale factors were periodically reduced by a randomly varied factor and then reincremented to their maximum values. Afterwards, structures were subjected to 200 steps of Powell minimization with NOE force constants at 20–40 kcal·mol$^{-1}$·Å$^{-2}$.

## 3. RESULTS AND DISCUSSION

ET-1 displays well-resolved sharp NMR resonances in 60% aqueous ethylene glycol. A downfield portion of the 160 ms NOESY at 295 K is shown in Fig. 1. All resonances of ET-1 spectra could be identified by a relatively straightforward application of the COSY/NOESY (i.e. spin correlation and nuclear Overhauser effect) strategy used for protein structures [22]. The use of two temperatures (295 K, 309 K) for the NOE spectroscopy was essential for the resolution of the extensive shift coincidences in the NH region. The aromatic δ hydrogens gave, in each case, an NOE connectivity to the corresponding Hα and/or Hβ resonances which were thus distinguished unambiguously. The corresponding Hδ/HN connectivities appear in Fig. 1. The same figure diagrams the (i, i+1) $d_{NN}$ connectivities from Lys$^9$ thru His$^{16}$. Unambiguous (i, i+1) $d_{\alpha N}$ connectivities link Cys$^1$→Lys$^6$ and Asp$^{18}$→Trp$^{21}$. The resulting chart of sequential connectivities appears in Fig. 2. Table I contains the complete resonance assignment. The five NOESY experiments afforded 220 conformationally dependent constraints with upper and lower bounds and more than 40 con-

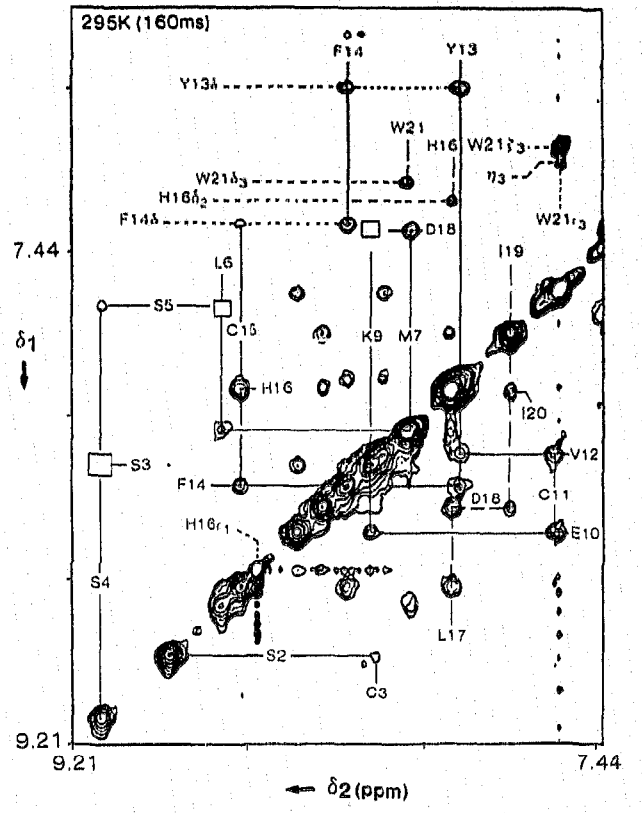


Fig. 1. NH/NH region of the NOESY spectrum ($\tau_m$ = 160 ms) of ET-1 (pH 3.2, at 295K). Backbone NH positions are solid or dashed lines labeled by residue number. The missing $d_{NN}$ connectivities are shown as empty boxes, the continuous solid lines trace the $d_{NN}$ connectivities from Ser$^4$ through His$^{16}$. Aromatic CH positions are shown by labeled dotted lines.

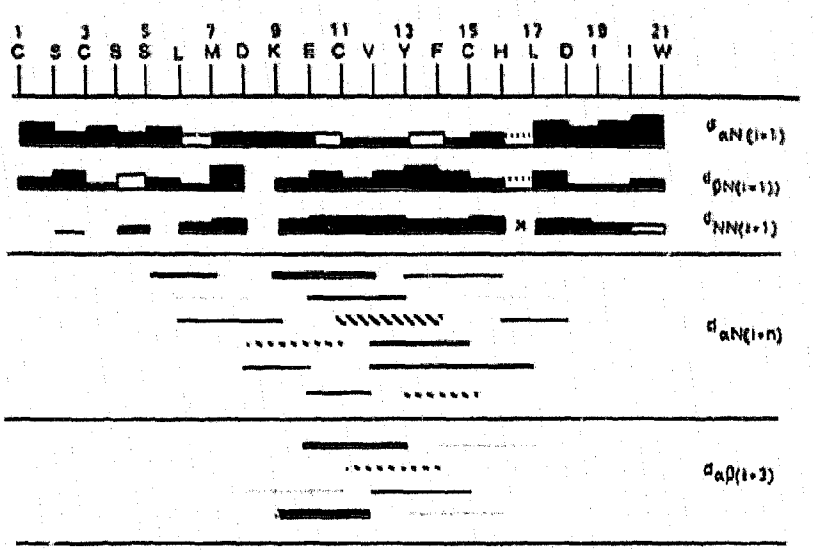


Fig. 2. Summary of the sequential connectivities. NOE intensities are shown by bar thickness: for the (i, i + 1) connectivities, an open bar indicates a potentially ambiguous assignment, an × indicates a shift coincidence prevents detection; for (i, i + n; n = 2-5) connectivities, a dashed line or bar indicates a probable assignment (used as a less weighted constraint in XPLOR), a dotted line indicates that a specific connectivity could be obscured by other peaks but is assumed absent (and excluded from all constraint lists).

straints with only lower bounds. The data set was reduced by deletion of constraints involving 19$\gamma$, 20$\gamma$, and 21$\beta$ protons, due to our lack of prochiral assignments, and conservative conversion of $\beta CH_2$ units to wildcard entries yielding 137 entries with upper and lower bounds and 31 entries with only a low bound. For the better-defined short distances ($r_{ij} < 3.1$ Å), bounds were as tight as ± 0.2 Å. The average range, $<r^{u}_{ij}-r^{l}_{ij}>$, for the full set of constraints was 0.74 Å.

Molecular dynamics simulation runs produced 68 final NMR structures using XPLOR, 9 structures using CONGEN, and 18 structures using DISCOVER. Six

Table I

Chemical shift assignment for endothelin at pH, 3.2[a]

| Residue | Chemical shift (ppm) | | | |
|---|---|---|---|---|
| | NH | $\alpha$ | $\beta,\beta'$ | others |
| C1 | ex | 4.33[b] | 3.30[c] | |
| S2 | 8.87 | 4.70 | 3.80 | |
| C3 | 8.18 | 5.05 | 3.21,2.49 | |
| S4 | 9.10 | 4.27 | 3.95,3.90 | |
| S5 | 7.62 | 4.56 | 3.96,3.66 | |
| L6 | 8.70 | 4.13 | 1.64,1.60 | $\gamma$ 1.68; $\delta$ 0.91,0.82 |
| M7 | 8.06 | 4.40 | 2.17,1.89 | $\gamma$ 2.61,2.45; $\epsilon$ 2.08 |
| D8 | 7.36 | 4.72 | 3.21[c],2.77[c] | |
| K9 | 8.20 | 3.86 | 1.85,1.81 | $\gamma$ 1.53,1.43; $\delta$ 1.68,1.64; $\epsilon$ 2.98,2.95 |
| E10 | 8.44 | 4.14 | 2.14 | $\gamma$ 2.49[c] |
| C11 | 7.59 | 4.22 | 3.20,3.12 | |
| V12 | 8.15 | 3.46 | 2.05 | $\gamma$ 0.98,0.83 |
| Y13 | 7.89 | 4.22 | 2.99,2.98 | $\gamma$ 6.84; $\epsilon$ 6.66 |
| F14 | 8.27[c] | 4.16 | 3.19,3.18 | $\delta$ 7.32; $\epsilon$ 7.35; $\zeta$ 7.28 |
| C15 | 8.64[c] | 4.58 | 3.26,2.94 | |
| H16 | 7.92 | 4.44 | 3.33[c],3.32[c] | $\delta_2$ 7.25[b]; $\epsilon_1$ 8.58[b] |
| L17 | 7.92 | 4.25 | 1.62,1.53 | $\gamma$ 1.52; $\delta$ 0.82,0.81 |
| D18 | 8.35 | 4.59 | 2.84[b],2.72[c] | |
| I19 | 7.72 | 4.10 | 1.70 | $\gamma_1$ 1.33,1.00; $\gamma_2$ 0.60; $\delta$ 0.78 |
| I20 | 7.94[c] | 4.16 | 1.77 | $\gamma_1$ 1.37,1.08; $\gamma_2$ 0.80; $\delta$ 0.79 |
| W21 | 8.08[b] | 4.63[c] | 3.29,3.18 | $\delta_1$ 7.17; $\epsilon_3$ 7.56; $\zeta_3$ 7.05 $\zeta_2$ 7.35; $\eta_2$ 7.11 |

[a]All shifts are $\delta$ values at 295K reported to the nearest ±0.01 ppm for 60% v/v ethylene glycol-$d_6$ $H_2O$. Resonances that undergo a substantial upfield shift upon adjusting the pH to 7 are highlighted: [b]$\Delta\delta > 0.20$, [c]$\Delta\delta = 0.08$–$0.20$ ppm. Some of the NH signals are shifted downfield at neutral pH, these are not highlighted.

Table II

Variation in Φ/Ψ averages (and rmsds) for the NOE refined structures

| Residue | Angle | CONGEN | DISCOVER | XPLOR | Selected* |
|---|---|---|---|---|---|
| 2 | Φ | -75(69) | -81(67) | -114(86) | -87(50) |
| | Ψ | 10(80) | 78(44) | 8(124) | 56(77) |
| 3 | Φ | -45(101) | -110(46) | -62(88) | -101(68) |
| | Ψ | 131(70) | 79(73) | 111(68) | 119(74) |
| 4 | Φ | -96(31) | -72(85) | -43(84) | -73(69) |
| | Ψ | 18(50) | 38(64) | 40(54) | 35(42) |
| 5 | Φ | -70(87) | -146(35) | 51(85) | -9(98) |
| | Ψ | 73(70) | 61(58) | 53(63) | 44(71) |
| 6 | Φ | -21(70) | -46(66) | -44(64) | -36(67) |
| | Ψ | 5(35) | -5(38) | 14(41) | 9(38) |
| 7 | Φ | -107(39) | -91(54) | -138(54) | -119(36) |
| | Ψ | -52(16) | -25(48) | -21(59) | -39(29) |
| 8 | Φ | -83(27) | -61(62) | -55(70) | -83(27) |
| | Ψ | 5(93) | -20(85) | 73(113) | 78(100) |
| 9 | Φ | -90(81) | -32(98) | 0(103) | -11(93) |
| | Ψ | 28(34) | 14(51) | -3(37) | 4(35) |
| 10 | Φ | -103(84) | -101(25) | -75(27) | -87(31) |
| | Ψ | -23(59) | -47(11) | -41(42) | -57(13) |
| 11 | Φ | -56(59) | -65(17) | -63(31) | -68(8) |
| | Ψ | -28(27) | -23(11) | -16(22) | -24(12) |
| 12 | Φ | -75(18) | -69(40) | -54(41) | -68(18) |
| | Ψ | -41(12) | -30(41) | -42(26) | -43(10) |
| 13 | Φ | -61(7) | -53(12) | -45(24) | -53(13) |
| | Ψ | -28(10) | -25(9) | -37(25) | -27(18) |
| 14 | Φ | -98(28) | -77(44) | -66(37) | -99(27) |
| | Ψ | -4(40) | -18(30) | -13(28) | -6(29) |
| 15 | Φ | -113(97) | -144(27) | -124(31) | -127(29) |
| | Ψ | -22(104) | -33(76) | -65(31) | -70(17) |
| 16 | Φ | -39(95) | -98(46) | -89(41) | -85(49) |
| | Ψ | -9(52) | 8(75) | -30(20) | -12(51) |
| 17 | Φ | -37(101) | -39(101) | -40(82) | -35(86) |
| | Ψ | 16(63) | 52(68) | 17(114) | -25(95) |
| 18 | Φ | -47(64) | -128(28) | -56(76) | -93(71) |
| | Ψ | 58(56) | 74(15) | 21(81) | 32(54) |
| 19 | Φ | -102(18) | -116(18) | -80(70) | -99(50) |
| | Ψ | 62(81) | 66(58) | 39(64) | -49(71) |
| 20 | Φ | -108(39) | -114(30) | -54(80) | -41(85) |
| | Ψ | -110(81) | 136(4) | -146(70) | -120(77) |

*Average of 16 selected structures (see text).

highly divergent starting structures were used, at least 4 of these were used in each protocol. None of the structures produced were disregarded in the analyses. Table II shows the variation in dihedral angles for all structures generated. It can be seen that the backbone conformation between residues 9–17 is essentially identical from the 3 protocols while the N- and C-termini show wider variations.

To allow for a normalized comparison of structures generated with the use of the CONGEN, DISCOVER and XPLOR force fields, selected models were relaxed to the local minimum using steepest descent minimization in CONGEN. Four CONGEN-, 5 DISCOVER- and 7 XPLOR-generated structures were selected based on: (1) an initial low average violation measure (<0.12 Å in XPLOR, and <0.25 Å in CONGEN and DISCOVER), and (2) acceptable energetics and fit to long range constraints after relaxation. Comparison of the 16 selected structures is the subject of Tables II and III and Fig. 3. The complete backbones for 5 selected structures appear in Fig. 4.

Tables II and Fig. 5B indicate that all 3 protocols produced a helical region between residues 9–17, however, the helix is not regular. All 3 protocols place the backbone torsion angles $\Psi_{11}$ and $\Psi_{14}$ at anomalous values near zero and open the helix at $\phi_{15}$ (circa -120°). For the N- and C-terminal regions data presented in Table II and Fig. 3 clearly suggest conformational averaging. However, a consensus turn-like structure emerges between residues 5–8 (Fig. 5A). Data in Table II also point to the 8/9 amide unit as a locus of conformational fluctuation ($\Psi_8$ and $\phi_9$). Similarly, the wide variance in $\phi/\Psi$ at Leu[17] suggests that this residue acts as a 'hinge' facilitating different orientations of the tail with respect to the rest of the molecule. The C-terminus does, however appear to be structured (cf. Fig. 1).

Table III

Average energies (in kcal) and surface characteristics of ET-1 models

| Comparison* | Dynamical simulation protocol | | |
|---|---|---|---|
| | CONGEN | DISCOVER | XPLOR |
| *Prior to relaxation* | | | |
| Ave. violation | | | |
| all 168 | 0.23 ± 0.03 | 0.21 ± 0.03 | 0.09 ± 0.01 |
| common 117 | 0.21 ± 0.04 | 0.15 ± 0.02 | 0.10 ± 0.02 |
| $E_{NOE}$ | 42.1 ± 2.3 | 53.3 ± 6.0 | 15.2 ± 2.0 |
| *After relaxation* | | | |
| $E_{total}$ | 15.4 ± 24.5 | 57.0 ± 13.2 | 94.4 ± 33.3 |
| $E_{bond}$ | 6.6 ± 0.4 | 7.0 ± 0.3 | 8.7 ± 1.3 |
| $E_{angle}$ | 109.7 ± 6.0 | 113.6 ± 4.3 | 141.1 ± 26.9 |
| $E_{non\text{-}bond}$ | -95.4 ± 11.9 | -81.9 ± 5.0 | -79.0 ± 8.6 |
| Ave. violation | | | |
| all 168 | 0.28 ± 0.02 | 0.27 ± 0.02 | 0.22 ± 0.02 |
| common 117 | 0.26 ± 0.03 | 0.24 ± 0.04 | 0.24 ± 0.02 |
| $E_{NOE}$ | 44.9 ± 4.5 | 62.3 ± 7.2 | 49.8 ± 4.3 |
| NP/P-SA | 4.89 ± 0.76 | 3.37 ± 0.22 | 5.00 ± 0.76 |

*The Ave. violation measures include that for the entire constraint set (all 168) and for only those constraints common to all 3 protocols (common 117), units are in Å. Constraints involving aromatic-Hδ and prochiral Leu-δMe, which cannot be used in CONGEN and DISCOVER, are excluded from the common 117 set. Energy terms were computed with CONGEN: $E_{NOE}$, interproton distance constraint energy (using the constraint set without aromatic Hδ and prochiral methyls), not included in $E_{total}$; $E_{bond}$, bond stretching term; $E_{angle}$ valence bond angle bending; $E_{non\text{-}bond}$, non-bonded interactions; $E_{total}$, total in vacuo energy including components of the CHARMM potential not listed here. The ratio of nonpolar/polar side chain solvent accessible surface (NP/P-SA), units are in Å.

Table III reveals that XPLOR-1.5 achieves its low levels of violation via large distortions of bond angles and large violations of repulsive van der Waal terms. After a common relaxation, all 3 protocols give structures with comparable fit to experimental constraints.

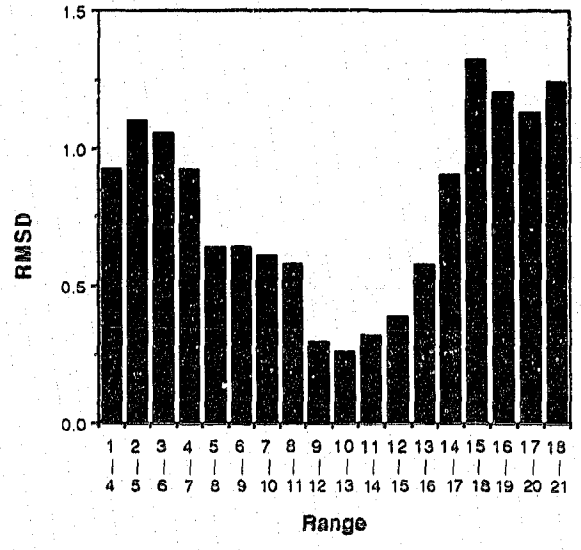


Fig. 3. Average root-mean-square deviation (RMSD) of backbone coordinates for the 16 selected structures taken pairwise. Using a window of 4 residues the RMSD of overlapping segments displaced from each other by one residue was calculated for each range.

Novotny et al. [23] and Chiche et al. [24] showed that the ratio of nonpolar/polar sidechain solvent accessiblity is a sensitive measure distinguishing native proteins from incorrectly folded models, with native proteins showing the maximum number of polar atoms exposed to the solvent. The non-polar/polar side-chain accessible surface ratio for ET-1 structures generated by DISCOVER are more favorable than those of CONGEN and XPLOR suggesting that DISCOVER generated structures that more closely resemble native proteins.

The ET-1 structural models derived in this paper have important physiological implications. It is known that the correct intact disulfide bonds are required for receptor binding and vasoconstrictor activity of ET-1 [25,26]. Other residues important for binding and biological activity are $Asp^{8}$, and $Glu^{10}$, $Phe^{14}$, and possibly $His^{16}$ and or $Asp^{18}$ [1,27–29]. It is interesting to see that the 2 disulfides are on one side of the helix (9–17) while the other side of the helix forms a contiguous area containing most of the above mentioned residues. Another side-chain implicated in biological activity is $Trp^{21}$ [25,28,29]. In our models, this residue is separated from the above active surface patch by flexible 'hinge' connecting the C-terminal tail to the rest of the molecule. In some accessible conformers this may place the C-terminus in a defined contact with the bicyclic core. A denser web of stereospecifically defined connectivities will be required to resolve this question.

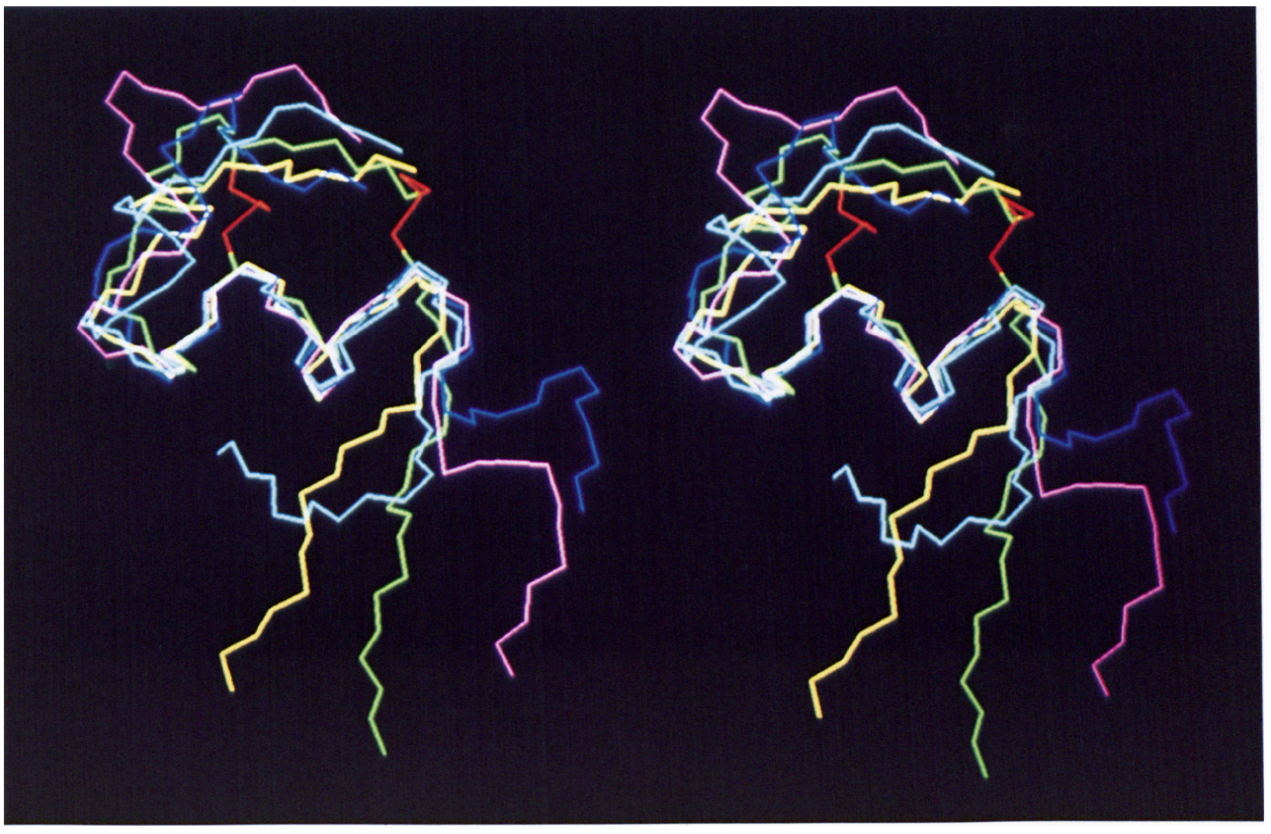

Fig. 4. Stereo view of the complete backbones for 5 of the selected structures superimposed for best fit of the helix (residues 9–16). Each structure is displayed in a different color with the two disulfides of one structure displayed in red.

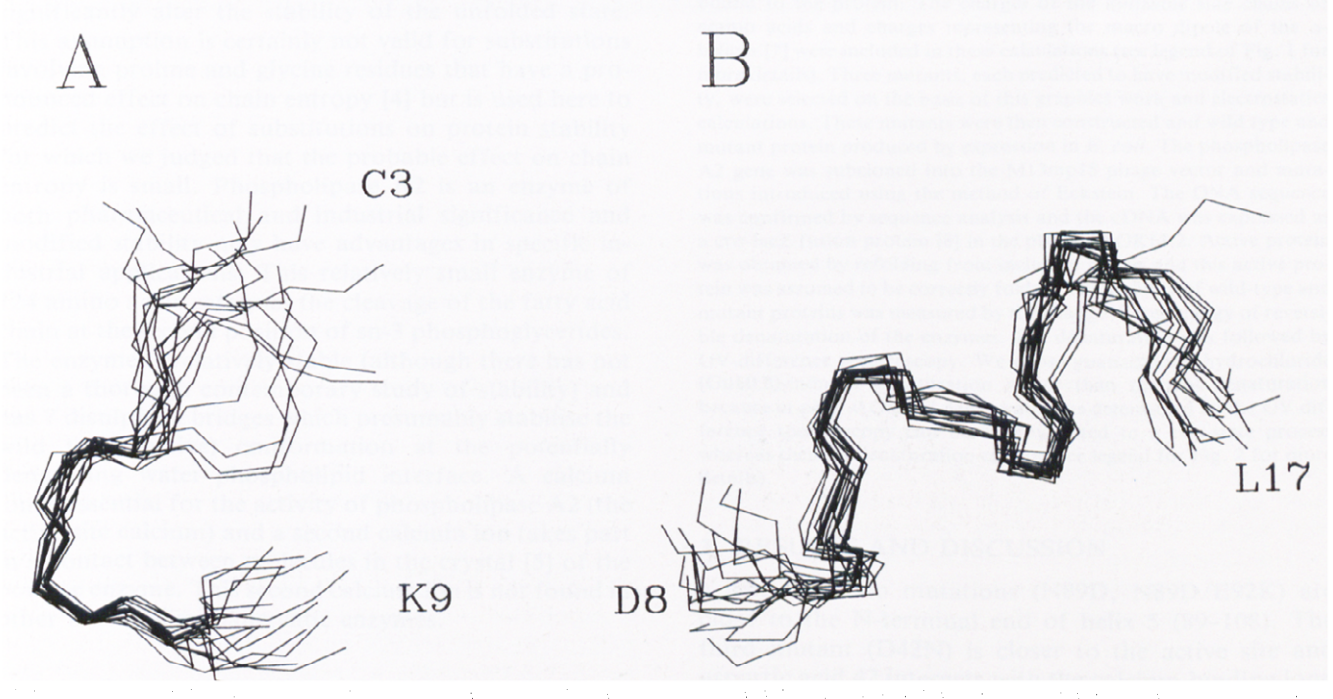


Fig. 5. Views (backbone atoms only) of the consensus structural elements of the 16 selected models. (A) Residues 3–9 are displayed with residues 5–8 superimposed showing the predominance of a turn-like conformation in this region of the peptide. (B) Residues 8–17 are displayed with residues 9–16 superimposed, demonstrating the presence of a helical region.

## REFERENCES


[1] Yanagisawa, M., Kurihara, H., Kimura, S., Tomobe, Y., Kobayashi, M., Mitsui, Y., Yazaki, Y., Goto, K. and Masaki, T. (1988) Nature 332, 411–415.
[2] Kloog, Y., Ambar, I., Sokolovsky, M., Kochva, E., Wollberg, Z. and Bdolah, A. (1988) Science 242, 268–270.
[3] Yanagisawa, M. and Masaki, T. (1989) TIPS 10, 374–378.
[4] Nayler, W.G. (1989) J. Appl. Physiol. 4, 495–503.
[5] Perkins, T.D.J., Hider, R.C. and Barlow, D.J. (1990) Int. J. Peptide Protein Res. 36, 128–133.
[6] Reily, M.D. and Dunbar, J.B. (1990) Abstract, IUPAB Satellite Symposium Whistler, British Columbia.
[7] Dalgarno, D., Senior, M., Slater, L. and Chackalamannil, S. (1990) Abstract, Eastern Analytical Symposium, Inc., Somerset, N.J.
[8] Saudek, V., Hoflack, J. and Pelton, J.T. (1989) FEBS Lett. 257, 145–148.
[9] Endo, S., Inooka, H., Ishibashi, Y., Kitada, C., Mizuta, E. and Fujino, M. (1989) FEBS Lett. 257, 149–154.
[10] Andersen, N.H., Lai, X. and Marschner, T. (1990) NOESYSIM/DISCON Documentation, copyrighted by the University of Washington; Lai, X., Chen, C. and Andersen, N.H., J. Magn. Reson. (in preparation).
[11] Clore, G.M., Appella, E., Yamada, M., Matsushima, K. and Gronenborn, A.M. (1990) Biochemistry 29, 1689–1700.
[12] Mueller, L. and Ernst, R.R. (1979) Mol. Phys. 38, 963–992.
[13] States, D.J., Haberkorn, R.A. and Ruben, D.J. (1982) J. Magn. Reson. 48, 286–292.
[14] Andersen, N.H., Eaton, H.L. and Nguyen, K.T. (1987) Mag. Reson. Chem. 25, 1025–1034.
[15] Marion, D. and Wuthrich, K. (1983) Biochem. Biophys. Res. Commun. 113, 967–974.
[16] Bruccoleri, R.E. and Karplus, M. (1987) Biopolymers 26, 137–168.
[17] Clore, G.M., Nilges, M., Sukumaran, D.K., Brunger, A.T., Karplus, M. and Gronenborn, A.M. (1986) EMBO J. 5, 2729–2735.
[18] Brooks, B., Bruccoleri, R.E., Olafson, B., States, D.J., Swaminathan, S. and Karplus, M. (1983) J. Comput. Chem. 4, 187–217.
[19] Bassolino, D.A., Novotny, J. and Bruccoleri, R.E. Manuscript in preparation.
[20] DISCOVER/INSIGHT Molecular Modeling Software, version 2.5, Biosym Technologies, San Diego, CA.
[21] XPLOR Molecular Modeling Software, version 1.5, Polygen Corp., Waltham, MA.
[22] Wuthrich, K. (1986) NMR of Proteins and Nucleic Acids, John Wiley and Sons, New York.
[23] Novotny, J., Rashin, A.A. and Bruccoleri, R.E. (1988) Proteins: Structure, Function, and Genetics 4, 19–30.
[24] Chiche, L., Gaboriaud, C., Heitz, A., Mornon, J.-P., Castro, B. and Kollman, P.A. (1989) Proteins: Structure, Function, and Genetics 6, 405–417.
[25] Kimura, S., Kasuya, Y., Sawamura, T., Shinmi, O., Sugita, Y., Yanagisawa, M., Goto, K. and Masaki, T. (1988) Biochem. Biophys. Res. Commun. 156, 1182–1186.
[26] Kumagaye, S.-I., Kuroda, H., Nakajima, K., Watanabe, T.X., Kimura, T., Masaki, T. and Sakakibara, S. (1988) Int. J. Pept. Protein Res. 32, 519–526.
[27] Nakajima, K., Kubo, S., Kumagaye, S.-I., Nishio, H., Tsunemi, M., Inui, T., Kuroda, H., Chino, N., Watanabe, T.X., Kimura, T. and Sakakibara, S. (1989) Biochem. Biophys. Res. Commun. 163, 424–429.
[28] Kitazumi, K., Shiba, T., Nishiki, K., Furukawa, Y., Takasaki, C. and Tasaka, K. (1990) FEBS Lett. 260, 269–272.
[29] Johansen, N.L., Lundt, B.F., Madsen, K., Olsen, U.B., Suzdak, P., Thogersen, H. and Weiss, J.U. (1990) Abstract, 21st European Peptide Symposium.